Nanoscale

Cite this: *Nanoscale*, 2012, **4**, 1078

www.rsc.org/nanoscale

PAPER

First-principles studies on structural and electronic properties of GaN–AlN heterostructure nanowires

Haijun Zhang,[ab] Yafei Li,[a] Qing Tang,[a] Lu Liu[a] and Zhen Zhou*[a]

Received 8th May 2011, Accepted 31st July 2011
DOI: 10.1039/c1nr10465a

The structural and electronic properties of core–shell, eutectic, biaxial and superlattice GaN–AlN nanowires were studied through density functional theory computations. Due to more surface dangling bonds, nanowires with smaller diameters are energetically unfavorable. For the GaN–AlN heterostructure nanowires, their electronic properties highly depend on the GaN content, axial strain, configuration, and size. The valence bands are less affected by the GaN content, while the conduction bands depend on it. Hydrogen-passivated nanowires have much larger band gaps than their counterparts, since the surface states are removed by saturating the dangling bonds with hydrogen atoms. Moreover, due to multiple quantum-well structures, the confined electrons (holes) of superlattice nanowires become more localized and the difference of the mobility between the electron and hole becomes less apparent if the width of the barrier is larger. These findings are of value for better understanding heterostructure nanowires and their potential utilization.

1. Introduction

Nanomaterials attract much attention due to their unique structure, and superior properties and applications in comparison with their bulk forms, among which nanowires (NWs) are very interesting with the charge carrier confined in a one-dimensional (1D) space owing to their special configuration. Semiconductor NWs represent unique systems for exploring phenomena at the nanoscale and are also expected to play a critical role in future electronic and optoelectronic devices. The range of potential applications of semiconductor NWs keeps increasing in the fields of optoelectronics,[1–3] device miniaturization,[4] field-effect transistors,[5–7] photovoltaic cells,[8–10] *etc.*

Component-modulated semiconductor heterostructures, such as core–shell, eutectic, biaxial, and superlattice types, are promising nanostructures, which not only offer the benefit of designing and fabricating nanodevices without further assembly, but also provide unique desirable properties for a variety of applications. Accordingly, in the past decades, efforts have been made in the synthesis, fabrication and simulation of heterostructure semiconductors, including group IV,[11–21] III–V,[22–30] and II–VI[31–40] heterostructure nanowires.

As two important members of the III–V semiconductor group, AlN and GaN have diverse properties and applications in electronics and photoelectronics, and tremendous progress has been made in their synthesis and fabrication.[41–45] However, pure nanowires can hardly satisfy the increasing demand for high-performance electronic and optoelectronic systems. The ability to control the electronic properties of nanowires by using band structure design in III–nitride radial nanowire heterostructures opens new opportunities for nanoelectronics and provides a new platform for low-dimensional physics.[46,47] In general, to meet the demand of different utilizations, the electronic structures of heterostructure nanowires can be tuned by changing the composition, configuration, and segment size. For the fabrication of nano-electronic devices based on GaN–AlN heterostructures, it is of great importance to understand the nature of spatial carrier confinement and the characteristics of band structures in various GaN–AlN heterostructure nanowires. However, previous theoretical studies[48–51] mostly focused on the structural, optical and electronic properties of pure AlN and GaN nanowires; there is little computational information on GaN–AlN heterostructures. In this work, by using density functional theory (DFT) computations, we systematically investigated the structural and electronic properties of core–shell, eutectic, biaxial, and superlattice GaN–AlN heterostructures, as well as the effects of surface H-passivation and axial strain, to look into their innate characteristics and provide a theoretical basis for their band structure engineering. The basic physics disclosed in this work is not constrained to GaN–AlN systems, but may be applicable to other semiconductor heterostructures.

2. Computational details

Our first-principles DFT computations were performed by using the plane-wave method implemented in the Vienna *ab initio*

[a]*Tianjin Key Laboratory of Environmental Remediation and Pollution Control, Institute of New Energy Material Chemistry, and Key Laboratory of Advanced Energy Materials Chemistry (Ministry of Education), Nankai University, Tianjin, 300071, P.R. China. E-mail: zhouzhen@nankai.edu.en*
[b]*School of Physics and Materials Science, Anhui University, Hefei, 230039, P.R. China*

simulation package (VASP).[52] The ion–electron interaction is described by the projector-augmented plane wave (PAW) approach.[53,54] The generalized gradient approximation (GGA) with the PW91 functional[55] and a 360 eV cutoff for the plane-wave basis set were adopted in all computations. To simulate infinitely long nanowire systems, a 1D periodic boundary condition (PBC) was applied along the growth direction of the nanowire. Our supercells are large enough to ensure that the vacuum space is at least 10 Å, so that the interaction between nanowires and their adjacent images can be safely avoided. Five Monkhorst–Pack special k points were used for sampling the 1D Brillouin zone, and the convergence threshold was set as 10^{-4} eV in energy and 10^{-3} eV Å^{-1} in force. On the basis of the equilibrium structures, 21 k points were then used to compute the band structures after geometry optimizations.

Both AlN and GaN nanowires usually adopt the wurtzite structure;[56,57] GaN–AlN heterostructures are thus created on the basis of wurtzite-structured nanowires and oriented along the [0001] direction. As shown in Fig. 1, all considered GaN–AlN heterostructure nanowires are oriented along the [0001] direction with the same cross-sectional hexagonal shape as the most stable AlN and GaN nanowires. While comparing the effects of different diameters and ratios of surface atoms, we take $(AlN)_{24}$, $(AlN)_{54}$, and $(AlN)_{96}$ as prototypes. The diameters of $(AlN)_{24}$, $(AlN)_{54}$, and $(AlN)_{96}$ are about 1.0 nm, 1.6 nm, and 2.2 nm, respectively. For GaN-core–AlN-shell (AlN-core–GaN-shell) nanostructures, we label them as $(GaN)_m@(AlN)_n$ [$(AlN)_n@(GaN)_m$] nanowires with m Ga–N pairs in the core (shell) region and n Al–N pairs in the shell (core) region. Meanwhile, the eutectic, biaxial, and superlattice NWs are labeled as eut(m,n), bia(m,n), and sl(m,n) composed of m Ga–N pairs and n Al–N pairs. The GaN content, x, is determined as $x = m/(m + n)$. The difference in x can be used to compare the effects of different compositions. For the core–shell nanowires with different GaN contents, the diameters are in the range of 1.0–2.2 nm, corresponding to the total atom number from 48 to 192 in the nanowires. The superlattice structures have the same diameter of 1.0 nm, but different segment lengths, including 96 and 192 atoms in a unit cell. The biaxial NWs, with diameters of 1.0 nm and 1.6 nm, have 48 and 108 atoms, respectively. We also considered the eutectic NWs, which have the same diameter of 1.0 nm but different GaN contents. The diameter of nanowires is defined by the average double distance from the center axis to the positions of the outmost atoms on the edge of the wires.

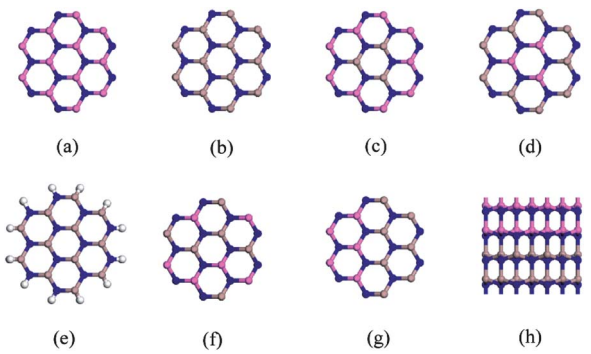

Fig. 1 (a)–(g) Represent top views of $(AlN)_{24}$, $(GaN)_{24}$, $(GaN)_6@(AlN)_{18}$, $(AlN)_6@(GaN)_{18}$, H passivated $(GaN)_{24}$, eutectic, and biaxial nanowires, respectively. (h) Is the side view of a superlattice nanowire. Brown, pink, blue, and white spheres represent Ga, Al, N, and H atoms, respectively.

3. Results and discussion

3.1. Geometry and structural stability of GaN–AlN heterostructure nanowires

After full relaxation of the atomic positions and lattice constants, there is a little inward and outward motion of the surface Al(Ga) and N atoms, respectively, as a result of the surface reconstruction. Accordingly, the length of Al(Ga)–N bonds in the zigzag side reduces by about 3% and the length of Al(Ga)–N bonds along the axial direction reduces by about 6%. The N–Al(Ga)–N and Al(Ga)–N–Al(Ga) bond angles increase and decrease, respectively, from the core to the surface. Taking the $(GaN)_6@(AlN)_{90}$ nanowire for an example, the N–Al–N and Al–N–Al bond angles become 118.5° and 106.6°, respectively (108.9° and 114.8° originally).

To evaluate the structural stability of GaN–AlN heterostructure nanowires, we calculated their formation energies. The formation energy (E_f) is defined as:[58]

$$E_f = (mE_{GaN} + nE_{AlN} - E_{tot})/(m + n) \quad (1)$$

where E_{AlN} and E_{GaN} is the energy of one Al–N pair in wurtzite AlN bulk and one Ga–N pair in wurtzite GaN bulk, respectively. E_{tot} is the total energy of the investigated nanostructures, m and n are the numbers of Ga–N and Al–N pairs in GaN–AlN heterostructures, respectively.

For the core–shell structures, the formation energies decrease obviously with increasing the nanowire diameters. The inversely proportional relationship between E_f and nanowire diameters (Fig. 2a) suggests that nanowires with larger sizes have higher stability. The result can be understood by the following reasons. Al(Ga) and N atoms prefer sp^3-hybridization in the wurtzite bulk in comparison with sp^2-hybridization in the surface of AlN (GaN) nanowires. Accordingly, the sp^2 hybridization is energetically unfavorable, which leads to the low stability. As a crucial factor determining the stability of the nanowires, the ratio of surface atoms has a functional relationship with the formation energy (Fig. 2b). E_f increases linearly with the ratio of surface atoms. Accordingly, thin nanowires with large ratios of surface atoms have high formation energies and they are very difficult to synthesize in experiments. In addition, $(GaN)_m@(AlN)_n$ [$(AlN)_n@(GaN)_m$] core–shell nanowires have similar stabilities to pure AlN (GaN) nanowires. With the same diameter, $(GaN)_m@(AlN)_n$ core–shell NWs have larger E_f's than $(AlN)_n@(GaN)_m$, which may be due to the surface Ga–N pairs of $(AlN)_n@(GaN)_m$ NWs. We also calculated the formation energies of eutectic, biaxial, and superlattice GaN–AlN heterostructure NWs with the same diameter of 1.0 nm. Because of the complicated configuration of eutectic NWs, we first calculated the formation energies of some different structures with the same GaN content and diameter, and then selected the configurations with the lowest formation energies (*i.e.* the most stable NWs). All eutectic, biaxial, and superlattice NWs have GaN contents of 0.25, 0.50, and 0.75. As shown in Fig. 3, with the same diameter,

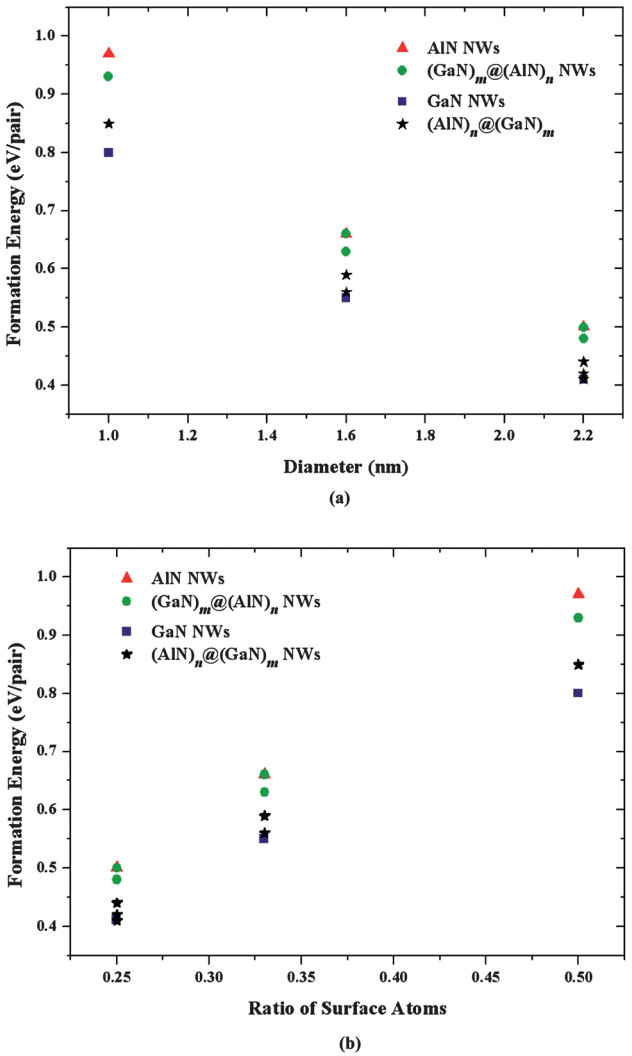

Fig. 2 Variation of formation energy with diameter (a) and ratio of surface atoms (b) for pure AlN (red triangle), $(GaN)_m@(AlN)_n$ (green circle), pure GaN (blue square), and $(AlN)_n@(GaN)_m$ core–shell (black star) nanowires.

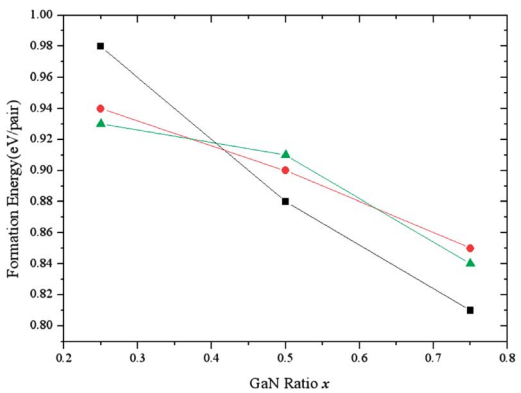

Fig. 3 Variation of formation energy with the GaN ratio x. Green triangles, red circles and black squares represent superlattice, biaxial and eutectic NWs with a diameter of 1.0 nm, respectively. The lines are guides for the eyes.

the formation energies of all the investigated heterostructures decrease with increasing GaN content, x. The GaN content has mild effects on the formation energies of nanowires. Therefore, the structural stability of nanowires is mainly affected by the diameters of nanowires, which dominate the level of dangling bonds.

3.2. Band structures of GaN–AlN heterostructure nanowires

In order to investigate the electronic properties of GaN–AlN heterostructure nanowires, we first computed the band structures of the optimized core–shell nanowires. The band structures of $(GaN)_m@(AlN)_n$ and $(AlN)_n@(GaN)_m$ ($m + n = 96$) core–shell nanowires are presented in Fig. 4. All the nanowires have direct gaps at the Γ point. Uniformly, all valence band maxima (VBM) are roughly flat and pinned around −0.5 eV, whereas the conduction band minima (CBM) of all the nanowires have parabolic shapes and different curvatures. The position of CBM drops with increasing GaN concentration, which is consistent with the results on CdSe nanoparticles,[59,60] indicating that the VBMs of GaN–AlN core–shell NWs with different sizes and GaN contents are also pinned relative to the Fermi level of the system. For a further investigation of the relationship between the GaN content and band gap, we computed the band structures of the eutectic, biaxial, and superlattice nanowires. Here we only computed the NWs with the diameter of 1.0 nm to economize resources.

As a matter of course, heterostructures with different configurations should have different band structures. However, the core–shell and eutectic (biaxial and superlattice) nanowires with the same diameter and GaN content have similar band structures. The biaxial and superlattice NWs have slightly smaller band gaps than the core–shell and eutectic NWs, which may be a result of interface effect. Taking the NWs with the same diameter (1.0 nm) and GaN content ($x = 0.25$) for an example,

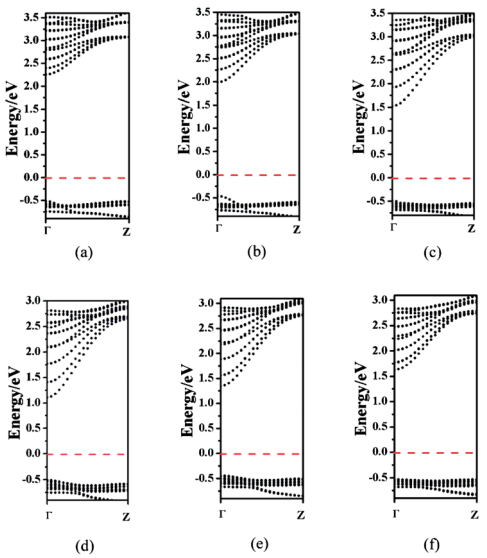

Fig. 4 (a–f) Band structures of $(GaN)_6@(AlN)_{90}$, $(GaN)_{24}@(AlN)_{72}$, $(GaN)_{54}@(AlN)_{42}$, $(AlN)_6@(GaN)_{90}$, $(AlN)_{24}@(GaN)_{72}$, and $(AlN)_{54}@(GaN)_{42}$ core–shell nanowires, respectively. Red dashed lines represent the Fermi level at 0 eV.

we find that the $(GaN)_6@(AlN)_{18}$ core–shell, eut(6,18), bia(6,18), and sl(24,72) NWs have band gaps of 2.44 eV, 2.48 eV, 2.31 eV, and 2.26 eV, respectively. Interestingly, the remarkable feature of superlattice nanowires is that all bands including the CBM and the VBM become flatter with the formation of minibands (see Fig. 5). The low curvature of band lines indicates a high effective mass and thus a small mobility of carrier. To investigate the effect of segment length on the electronic properties of the superlattice NWs, we computed sl(48,48) with the same diameter as sl(24,24), which have a double segment length of sl(24,24). Due to the additional minibands, both CBM and VBM become flatter as the segment length increases and the band gap decreases with increasing the segment length. These geometry effects on the electronic properties of the superlattice nanowires can be well understood by a multiple quantum well structure.[61] Because the conduction and valence band edges of different regions (AlN and GaN regions) in the superlattice nanowires have different energies, the diagram of CBM and VBM along the axis of superlattice NWs will display a multiple quantum well structure according to the Kronig–Penney model. Electrons in the well region of a zone should decay in the adjacent zones having a higher CBM, since their energy will fall into the band gap of this barrier zone. As a result, the states of these confined electrons are propagating in the well but decaying in the barrier. Because of their low group velocity, the confined electrons may become more localized if the barrier is high and the width of barrier is large.

Moreover, what about the relationship between band gaps and diameters? The bia(27,27) nanowire with a diameter of 1.6 nm has a direct gap of 1.84 eV, which is smaller than that (2.00 eV) of bia(12,12) with a diameter of 1.0 nm. $(AlN)_6@(GaN)_{18}$ nanowire has a smaller diameter (1.0 nm) and larger band gap (2.01 eV), while $(AlN)_{24}@(GaN)_{72}$ nanowire with a diameter of 2.2 nm shows a band gap of 1.78 eV. These results precisely confirm the size effect.

The band gaps of both $(GaN)_m@(AlN)_n$ and $(AlN)_n@(GaN)_m$ core–shell nanowires vary inversely with the GaN content x, as shown in Fig. 6a. Moreover, the band gaps of eutectic, biaxial, and superlattice NWs with the same diameter also decrease with the increase in GaN content x (see Fig. 6b)]. For confirmation, we computed the band structures of bulk AlN and GaN. As expected, the GaN bulk has a smaller band gap (2.59 eV) than AlN bulk (4.39 eV). Therefore, we can draw a conclusion that the band gaps of all GaN–AlN heterostructure NWs vary inversely with the GaN content.

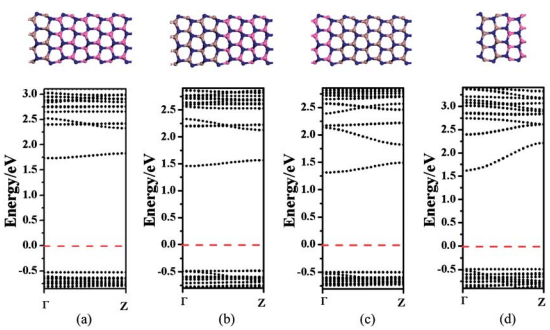

Fig. 5 Band structures and optimized geometries of (a) sl(24,72), (b) sl (48,48), (c) sl(72,24), and (d) sl(24,24) NWs. Red dashed lines represent the Fermi level at 0 eV.

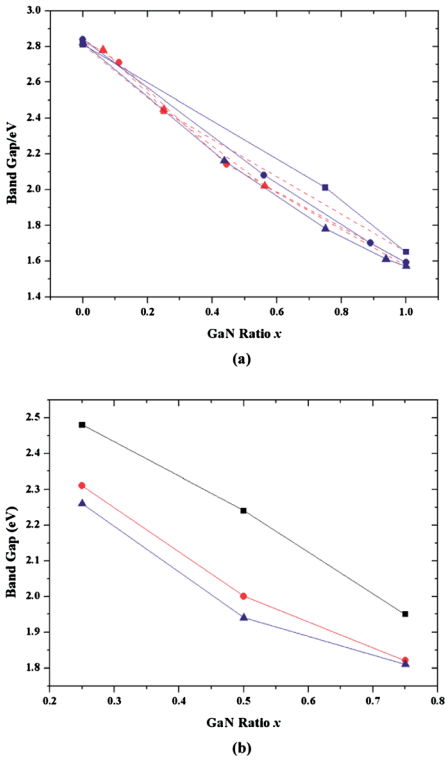

Fig. 6 Variations of the direct band gap E_g as a function of the GaN content x [$x = m/(m + n)$] for (a) $(GaN)_m@(AlN)_n$ (red dashed line) and $(AlN)_n@(GaN)_m$ (blue solid line) core–shell nanowires with different numbers of atoms in the unit cell: 48 (squares), 108 (circles) and 196 (triangles), and (b) eutectic (black squares), biaxial (red circles), and superlattice (blue triangles) heterostructure GaN–AlN nanowires with 48 atoms in the unit cell. The lines are guides for the eyes.

For further understanding of the surface effects, we investigated the hydrogenated $(GaN)_6@(AlN)_{18}$ core–shell, $(AlN)_6@(GaN)_{18}$ core–shell, eut(12,12), bia(12,12), and sl(24,24) heterostructure NWs. As shown in Fig. 7, the H-passivated NWs are still direct band gap semiconductors with VBMs pinned around −0.5 eV. Nevertheless, the CBMs of the investigated NWs are enhanced a lot after hydrogenation, resulting in much larger gaps of H-passivated NWs than those of the counterparts. For instance, as shown in Fig. 7a and f, bare $(GaN)_6@(AlN)_{18}$ has a band gap of 2.44 eV, while the band gap of H-passivated $(GaN)_6@(AlN)_{18}$ is 4.21 eV. As expected, the passivation of the exposed bonds with hydrogen removes the surface states, which give the dominant contribution to the band gap of bare GaN–AlN heterostructure NWs.

We also investigated the strain effect on the electronic properties of GaN–AlN heterostructures, which was performed under a constant unit cell with volume constraint, and the axial unit cell length c is determined by the percentage strain α ($c = c_0(1 + \alpha)$), where c_0 is the unit cell length of the optimized, unstrained nanowire. It can be seen from Fig. 8 that the band gap of all heterostructures varies inversely with the absolute value of α, when α changes from −5% to 5%. Except the biaxial nanowire whose band gap increases under 2.5% tension (probably due to

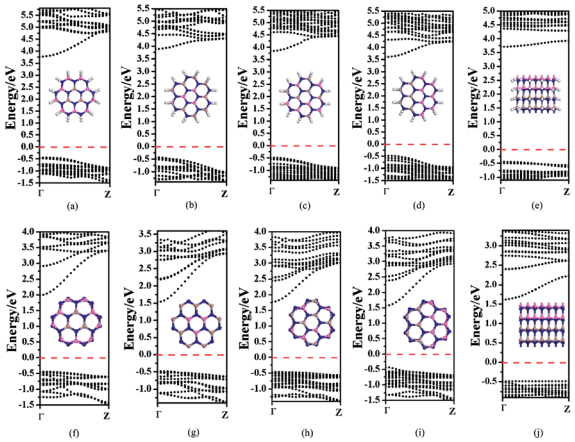

Fig. 7 Band structures and optimized geometries of H-passivated (unpassivated) heterostructures. (a)–(e) [(f)–(j)] represent H-passivated (bare) $(GaN)_6@(AlN)_{18}$ core–shell, $(AlN)_6@(GaN)_{18}$ core–shell, eut (12,12), bia(12,12), and sl(24,24) NWs, respectively. Red dashed lines represent the Fermi level at 0 eV. Fully-relaxed structures are inserted into the blank space of band structures.

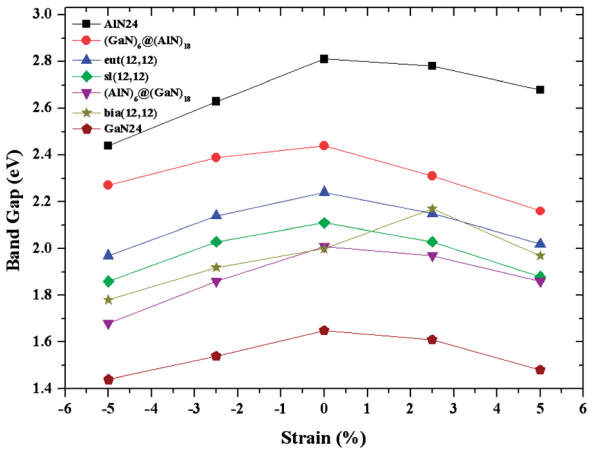

Fig. 8 Variation of band gaps with axial strain.

the interface change), all heterostructures have decreasing band gaps with increasing strain. Therefore, both compression and tension reduce the band gap of GaN–AlN heterostructure nanowires.

It is well known that DFT underestimates the band gaps of semiconductors, but the variation tendency is reliable and valuable.

3.3. Charge distribution of CBMs and VBMs for GaN–AlN heterostructure nanowires

To further clarify the electronic properties of GaN–AlN heterostructure nanowires, we calculated the spatial localizations of the VBMs and the CBMs of core–shell, eutectic, biaxial, superlattice, and hydrogenated nanowires, which are shown in Fig. 9–12. The CBMs and VBMs are distributed variously, which depend on the configuration of nanowires. For core–shell NWs, with a given diameter of 2.2 nm, the CBM distribution is mainly located in the GaN region at high GaN contents (see Fig. 9b–e) and composed

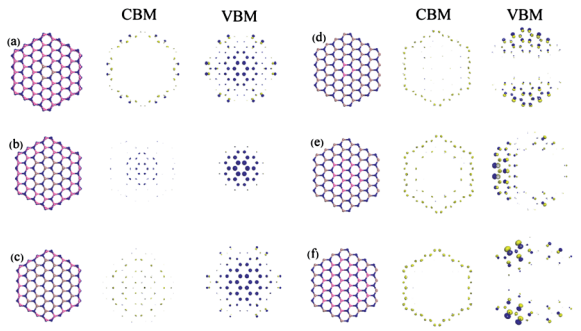

Fig. 9 CBM and VBM charge density of the core–shell nanowires with the diameter of 2.2 nm. The relaxed structures are given on the left.

of N s states, while it is located in the AlN region at low GaN contents (see Fig. 9a) and mainly composed of surface Al and N *s* states. For the core–shell NWs with a diameter of 1.6 nm, we can obtain similar results. Otherwise, the distribution of VBMs spreads over the entire NWs, except $(GaN)_{24}@(AlN)_{72}$ and $(AlN)_{24}@(GaN)_{72}$ NWs, and all the nanowires with different GaN contents have the VBMs dominated by the p states from inner or outer N atoms. As we can see from the above feature, the band gaps of nanowires with high concentrations of GaN are mostly dominated by the GaN gap and decrease with increasing the GaN ratio *x*.

Moreover, for $(GaN)_{24}@(AlN)_{72}$ and $(AlN)_{24}@(GaN)_{72}$ NWs with a core radius of 0.5 nm and shell thickness of 0.6 nm, both the VBM and CBM distribution are located in the GaN region. This observation may be a result of confined states of core–shell structure nanowires with a proper core and shell thickness.[62]

As shown in Fig. 10, all the CBMs of eutectic NWs are spread all around the NWs. However, the CBMs of eut(6,18) and eut (18,6) NWs are mainly composed of N s states and surface Al and Ga *s* states, but the CBM distribution of eut(12,12) NW is mainly composed of the N s states and surface Ga s states. Similarly, the VBMs of eutectic NWs spread all over the NWs, which are composed of N p states. For biaxial NWs, the distribution of CBMs and VBMs are mostly located in the GaN region, which may be affected by the interface between the GaN and AlN region. The CBMs of both NWs are composed of N s states and surface Ga s states, and the VBMs of them are composed of N p states. That is why the eutectic NWs have larger band gaps than biaxial NWs, as shown in Fig. 6b.

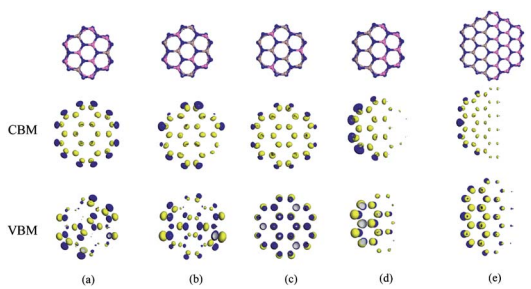

Fig. 10 CBM and VBM distribution of eutectic (a–c) and biaxial (d, e) NWs. The optimized structures are also given.

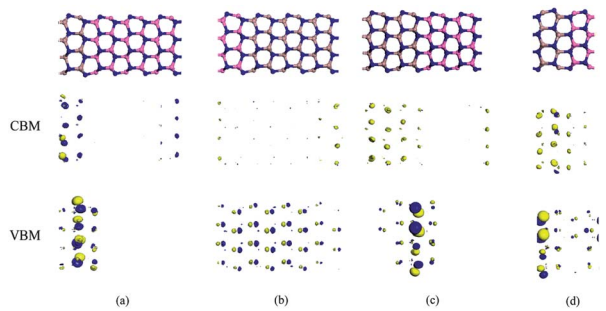

Fig. 11 (a–d) CBM and VBM distribution of sl(24,72), sl(72,24), sl (48,48), and sl(24,24) NWs, respectively.

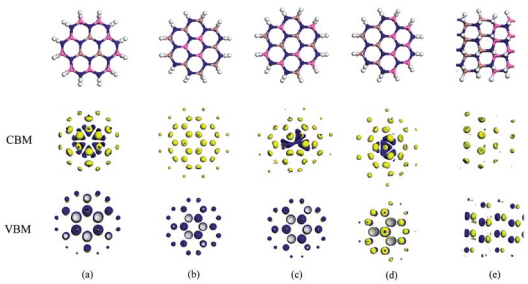

Fig. 12 (a)–(e) represent the optimized geometries and spatial distributions of the VBM and CBM states at the Γ point for H-passivated $(GaN)_6@(AlN)_{18}$ core–shell, $(AlN)_6@(GaN)_{18}$ core–shell, eut(12,12), bia (12,12), and sl(24,24) NWs, respectively.

From Fig. 11 we can see that the CBMs are mainly distributed on N atoms (s states) in the GaN region, and the distributions of VBMs are localized on N atoms (p states) in the interface region. Therefore, the electronic properties of superlattice GaN–AlN NWs are primarily determined by the N atoms in the GaN region and highly depend on the multiple quantum well structure. Other atoms in AlN region make little contribution to either the VBM or CBM.

As shown in Fig. 12, all VBMs of hydrogenated NWs are composed of N p states and are mainly distributed in the interior of the NWs, owing to the saturated surface exposed bonds. As a result of passivation, the CBMs of passivated NWs are mostly located on the interior atoms, which are composed of N s states. Interestingly, there are contributions of Ga d states for the CBMs of H-passivated $(GaN)_6@(AlN)_{18}$ core–shell, eut(12,12) and bia (12,12) NWs. This may be a result of the high densities of Ga atoms in the interior region, as shown in Fig. 12a, c, and d. As for the biaxial and superlattice NWs, the saturation of surface exposed bonds weakens the surface effect and the CBMs and VBMs tend to spread over the entire NWs.

4. Conclusion

In summary, we have investigated the structural stability and electronic properties of GaN–AlN core–shell, eutectic, biaxial and superlattice heterostructure nanowires through first-principles computations. The formation energy of nanowires is dominated by the ratio of surface atoms which is inversely proportional to the diameter. All the studied heterostructure nanowires have wide direct band gaps. For GaN–AlN heterostructures, the GaN content, axial strain, geometric configuration, and size have important effects on the electronic properties. The valance band edges are less affected by the GaN content while the conduction band edges decrease with the increase in GaN concentration. For all the investigated nanowires, the band gaps are mainly dominated by the GaN content. With a proper core size and shell thickness, quantum confined states of electrons and holes in the core region are obtained. For eutectic, biaxial, and superlattice GaN–AlN nanowires, the electronic properties are primarily determined by their configuration as expected. With regard to the superlattice nanowires, the confined states that offer promising device applications are clearly demonstrated by the isosurface plots of charge densities. The confined electrons (holes) become more localized and the associated bands become flatter if the width of the barrier is larger. The computations on H-passivated structures demonstrate that the electronic properties of GaN–AlN nanowires highly depend on the surface states. The results and principles disclosed in this work may be adapted to other semiconductor heterostructures for band structure engineering and nanodevice designing.

Acknowledgements

This work was supported by NSFC (20873067), MOE NCET (08-0293) and the Innovation Team (IRT0927) in China.

Notes and References

1 X. F. Duan, Y. Huang, Y. Cui, J. F. Wang and C. M. Lieber, *Nature*, 2001, **409**, 66.
2 T. Someya, R. Werner, A. Forchel, M. Catalano, R. Cingolani and Y. Arakawa, *Science*, 1999, **285**, 1905.
3 J. C. Johnson, H.-J. Choi, K. P. Knutsen, R. D. Schaller, P. D. Yang and R. J. Saykally, *Nat. Mater.*, 2002, **1**, 106.
4 Y. Huang, X. F. Duan, Y. Cui, L. J. Lauhon, K.-H. Kim and C. M. Lieber, *Science*, 2001, **294**, 1313.
5 Y. Cui, Z. H. Zhong, D. L. Wang, W. U. Wang and C. M. Lieber, *Nano Lett.*, 2003, **3**, 149.
6 J. Xiang, W. Lu, Y. J. Hu, Y. Wu, H. Yan and C. M. Lieber, *Nature*, 2006, **441**, 489.
7 A. L. Vallett, S. Minassian, P. Kaszuba, S. Datta, J. M. Redwing and T. S. Mayer, *Nano Lett.*, 2010, **10**, 4813.
8 A. Hagfeldt and M. Grätzel, *Chem. Rev.*, 1995, **95**, 49.
9 B. Z. Tian, X. L. Zheng, T. J. Kempa, Y. Fang, N. F. Yu, G. H. Yu, J. L. Huang and C. M. Lieber, *Nature*, 2007, **449**, 885.
10 M. R. Lee, R. D. Eckert, K. Forberich, G. Dennler, C. J. Brabec and R. A. Gaudiana, *Science*, 2009, **324**, 232.
11 L. J. Lauhon, M. S. Gudiksen, D. L. Wang and C. M. Lieber, *Nature*, 2002, **420**, 57.
12 H. Peelaers, B. Partoens and F. M. Peeters, *Phys. Rev. B: Condens. Matter Mater. Phys.*, 2010, **82**, 113411.
13 R. Peköz and J.-Y. Raty, *Phys. Rev. B: Condens. Matter Mater. Phys.*, 2009, **80**, 155432.
14 X. J. Hao, T. Tu, G. Cao, C. Zhou, H. O. Li, G. C. Guo, W. Y. Fung, Z. Q. Ji, G. P. Guo and W. Lu, *Nano Lett.*, 2010, **10**, 2956.
15 X. Chen, Y. C. Wang and Y. M. Ma, *J. Phys. Chem. C*, 2010, **114**, 9096.
16 X. H. Peng and P. Logan, *Appl. Phys. Lett.*, 2010, **96**, 143119.
17 R. N. Musin and X. Q. Wang, *Phys. Rev. B: Condens. Matter Mater. Phys.*, 2006, **74**, 165308.
18 R. N. Musin and X. Q. Wang, *Phys. Rev. B: Condens. Matter Mater. Phys.*, 2005, **71**, 155318.
19 K. M. Varahramyan, D. Ferrer, E. Tutuc and S. K. Banerjee, *Appl. Phys. Lett.*, 2009, **95**, 033101.
20 N. Akman, E. Durgun, S. Cahangirov and S. Ciraci, *Phys. Rev. B: Condens. Matter Mater. Phys.*, 2007, **76**, 245427.
21 C. Dames and G. Chen, *J. Appl. Phys.*, 2004, **95**, 682.

22 X. C. Jiang, Q. H. Xiong, S. Nam, F. Qian, Y. Li and C. M. Lieber, *Nano Lett.*, 2007, **7**, 3214.
23 M. A. Verheijen, R. E. Algra, M. T. Borgström, G. Immink, E. Sourty, W. J. P. V. Enckevort, E. Vlieg and E. P. A. M. Bakkers, *Nano Lett.*, 2007, **7**, 3051.
24 P. Krogstrup, J. Yamasaki, C. B. Sørensen, E. Johnson, J. B. Wagner, R. Pennington, M. Aagesen, N. Tanaka and J. Nygård, *Nano Lett.*, 2009, **9**, 3689.
25 Y. Li, J. Xiang, F. Qian, S. Gradečak, Y. Wu, H. Yan, D. A. Blom and C. M. Lieber, *Nano Lett.*, 2006, **6**, 1468.
26 Y. J. Dong, B. Z. Tian, T. J. Kempa and C. M. Lieber, *Nano Lett.*, 2009, **9**, 2183.
27 D. C. Mojica and Y. M. Niquet, *Phys. Rev. B: Condens. Matter Mater. Phys.*, 2010, **81**, 195313.
28 A. Nduwimana, R. N. Musin, A. M. Smith and X. Q. Wang, *Nano Lett.*, 2008, **8**, 3341.
29 Y. M. Niquet, *Nano Lett.*, 2007, **7**, 1105.
30 H. B. Shu, X. S. Chen, X. H. Zhou and W. Lu, *Chem. Phys. Lett.*, 2010, **495**, 261.
31 J. Yan, X. S. Fang, L. D. Zhang, Y. Bando, U. K. Gautam, B. Dierre, T. Sekiguchi and D. Golberg, *Nano Lett.*, 2008, **8**, 2794.
32 Y. Tak, S. J. Hong, J. S. Lee and K. Yong, *Cryst. Growth Des.*, 2009, **9**, 2627.
33 Y. Tak, S. J. Hong, J. S. Lee and K. Yong, *J. Mater. Chem.*, 2009, **19**, 5945.
34 K. Wang, J. J. Chen, Z. M. Zeng, J. Tarr, W. L. Zhou, Y. Zhang, Y. F. Yan, C. S. Jiang and J. Pern, *Appl. Phys. Lett.*, 2010, **96**, 123105.
35 M.-Y. Lu, J. H. Song, M.-P. Lu, C.-Y. Lee, L.-J. Chen and Z. L. Wang, *ACS Nano*, 2009, **3**, 357.
36 H. Pan and Y. P. Feng, *ACS Nano*, 2008, **2**, 2410.
37 J. Schrier, D. O. Demchenko and L. W. Wang, *Nano Lett.*, 2007, **7**, 2377.
38 X. Fan, M. L. Zhang, I. Shafiq, W. J. Zhang, C.-S. Lee and S.-T. Lee, *Adv. Mater.*, 2009, **21**, 2393.
39 S. Y. Yang, D. Prendergast and J. B. Neaton, *Nano Lett.*, 2010, **10**, 3156.
40 Z. J. Jiang and D. F. Kelley, *J. Phys. Chem. C*, 2010, **114**, 17519.
41 Q. Zhao, H. Z. Zhang, X. Y. Xu, Z. Wang, J. Xu, D. P. Yu, G. H. Li and F. H. Su, *Appl. Phys. Lett.*, 2005, **86**, 193101.
42 H. M. Huang, R. S. Chen, H. Y. Chen, T. W. Liu, C. C. Kuo, C. P. Chen, H. C. Hsu, L. C. Chen, K. H. Chen and Y. J. Yang, *Appl. Phys. Lett.*, 2010, **96**, 062104.
43 T. Kuykendall, P. J. Pauzauskie, Y. F. Zhang, J. Goldberger, D. Sirbuly, J. Denlinger and P. D. Yang, *Nat. Mater.*, 2004, **3**, 524.
44 C.-T. Huang, J. H. Song, W.-F. Lee, Y. Ding, Z. Y. Gao, Y. Hao, L.-J. Chen and Z. L. Wang, *J. Am. Chem. Soc.*, 2010, **132**, 4766.
45 Y. Huang, X. F. Duan, Y. Cui and C. M. Lieber, *Nano Lett.*, 2002, **2**, 101.
46 Y. Li, J. Xiang, F. Qian, S. Gradečak, Y. Wu, H. Yan, D. A. Blom and C. M. Lieber, *Nano Lett.*, 2006, **6**, 1468.
47 L. Rigutti, M. Tchernycheva, A. D. L. Bugallo, G. Jacopin, F. H. Julien, L. F. Zagonel, K. March, O. Stephan, M. Kociak and R. Songmuang, *Nano Lett.*, 2010, **10**, 2939.
48 (*a*) M. W. Zhao, Y. Y. Xia, X. D. Liu, Z. Y. Tan, B. D. Huang, C. Song and L. M. Mei, *J. Phys. Chem. B*, 2006, **110**, 8764; (*b*) Z. Zhou, J. J. Zhao, Y. S. Chen, Z. F. Chen and P. v. R. Schleyer, *Nanotechnology*, 2007, **18**, 424023.
49 Y. F. Li, Z. Zhou, P. W. Shen, S. B. Zhang and Z. F. Chen, *Nanotechnology*, 2009, **20**, 215701.
50 Y. F. Li, Z. Zhou, Y. S. Chen and Z. F. Chen, *J. Chem. Phys.*, 2009, **130**, 204706.
51 D. J. Carter, J. D. Gale, B. Delley and C. Stampfl, *Phys. Rev. B: Condens. Matter Mater. Phys.*, 2008, **77**, 115349.
52 G. Kresse and J. Hafner, *Phys. Rev. B: Condens. Matter*, 1994, **49**, 14251.
53 P. E. Blöchl, *Phys. Rev. B: Condens. Matter*, 1994, **50**, 17953.
54 G. Kresse and D. Joubert, *Phys. Rev. B: Condens. Matter Mater. Phys.*, 1999, **59**, 1758.
55 J. P. Perdew and Y. Wang, *Phys. Rev. B: Condens. Matter*, 1992, **45**, 13244.
56 L. H. Shen, X. F. Li, J. Zhang, Y. M. Ma, F. Wang, G. Peng, Q. L. Cui and G. T. Zou, *Appl. Phys. B*, 2006, **8**, 73.
57 C. C. Chen, C. C. Yeh, C. H. Chen, M. Y. Yu, H. L. Liu, J. J. Wu, K. H. Chen, L. C. Chen, J. Y. Peng and Y. F. Chen, *J. Am. Chem. Soc.*, 2001, **123**, 2791.
58 H. B. Shu, X. S. Chen, H. X. Zhao, X. H. Zhou and W. Lu, *J. Phys. Chem. C*, 2010, **114**, 17514.
59 B. Carlson, K. Leschkies, E. S. Aydil and X. Y. Zhu, *J. Phys. Chem. C*, 2008, **112**, 8419.
60 T. Z. Markus, M. Wu, L. Wang, D. H. Waldeck, D. Oron and R. Naaman, *J. Phys. Chem. C*, 2009, **113**, 14200.
61 N. Akman, E. Durgun, S. Cahangirov and S. Ciraci, *Phys. Rev. B: Condens. Matter Mater. Phys.*, 2007, **76**, 245427.
62 L. Yang, R. N. Musin, X. Q. Wang and M. Y. Chou, *Phys. Rev. B: Condens. Matter Mater. Phys.*, 2008, **77**, 195325.

